Seasonal variation of fine- and coarse-mode nitrates and related aerosols over East Asia: Synergetic observations and chemical transport model analysis

Itsushi Uno[1], Kazuo Osada[2], Keiya Yumimoto[1], Zhe Wang[1,3], Syuichi Itahashi[4],

5 Xiaole Pan[3], Yukari Hara[1], Yugo Kanaya[5], Shigekazu Yamamoto[6], Thomas Duncan Fairlie[7]

[1] Research Institute for Applied Mechanics, Kyushu University, Kasuga Park 6-1, Fukuoka 816-8580, Japan

[2] Nagoya University, Graduate School of Environ. Studies, Furo-cho, Chikusa-ku, Nagoya, 464-8601, Japan

[3] Institute of Atmospheric Physics, CAS, Beijing, China

[4] Central Research Institute of Electric Power Industry, Abiko, Chiba, 270-1194, Japan

10 [5] Japan Agency for Marine-Earth Science and Technology, 3173-25 Showa-machi, Kanazawa-ku, Yokohama, 236-0001, Japan

[6] Fukuoka Institute of Health and Environmental Sciences, Mukaizano 39, Dazaifu, Fukuoka 818-0135, Japan

[7] NASA, Langley Research Center, Hampton, VA 23681-0001, U.S.A.

15 *Correspondence to*: Itsushi Uno (uno@riam.kyushu-u.ac)

Abstract. We analyzed long-term fine- and coarse-mode synergetic observations of nitrate and related aerosols (SO_4^{2-}, NO_3^-, NH_4^+, Na^+, Ca^{2+}) at Fukuoka (33.52°N, 130.47°E) from August 2014 to October 2015. A Goddard Earth Observing System chemical transport model (GEOS-Chem) including dust and sea-salt acid uptake processes was used to assess the observed seasonal variation and the impact of long-range transport (LRT) from the Asian continent. For fine aerosols (fSO_4^{2-}, fNO_3^-,

20 and fNH_4^+), numerical results explained the seasonal changes, and a sensitivity analysis excluding Japanese domestic emissions clarified the LRT fraction at Fukuoka (85% for fSO_4^{2-}, 47% for fNO_3^-, 73% for fNH_4^+). Observational data confirmed that coarse NO_3^- (cNO_3^-) made up the largest proportion (i.e., 40–55%) of the total nitrate (defined as the sum of fNO_3^-, cNO_3^- and HNO_3) during the winter, while HNO_3 gas constituted approximately 40% of the total nitrate in summer, and fNO_3^- peaked during the winter. Large-scale dust-nitrate (mainly cNO_3^-) outflow from China to Fukuoka was confirmed

25 during all dust events that occurred between January and June. The modeled cNO_3^- was in good agreement with observations between July and November (mainly coming from sea salt-NO_3^-). During the winter, however, the model underestimated cNO_3^- levels compared to the observed levels. The reason for this underestimation was examined statistically using multiple regression analysis (MRA). We used cNa^+, $nss-cCa^{2+}$, and cNH_4^+ as independent variables to describe the observed cNO_3^- levels; these variables were considered representative of sea salt-cNO_3^-, dust-cNO_3^-, and cNO_3^- accompanied by cNH_4^+

30 (cNH_4^+ term), respectively. The MRA results explained the observed seasonal changes in dust-cNO_3^- and indicated that the dust-acid uptake scheme reproduced the observed dust-nitrate levels even in winter. The annual average contributions of each component were 43% (sea salt-cNO_3^-), 19% (dust cNO_3^-), and 38% (cNH_4^+ term). The MRA dust-cNO_3^- component had a high value during the dust season, and the sea salt component made a large contribution throughout the year. During the

winter, cNH_4^+ term made a large contribution. The model did not include aerosol microphysical processes (such as condensation and coagulation between the fine anthropogenic aerosols NO_3^- and SO_4^{2-} and coarse particles), and our results suggest that inclusion of aerosol microphysical processes is critical when studying observed cNO_3^- formation, especially in winter.

1 Introduction

Long-range trans-boundary transport of dust and pollutants in East Asia, and their complex interactions, are an important environmental issue due to the recent rapid economic developments and changes in these areas (e.g., Lawrence and Lelieveld, 2010, Li *et al.* 2017, Zhang *et al.*, 2017). Because of the heavy air pollution occurring in China, a great deal of research
10   focuses mainly on fine-mode aerosols (i.e., $PM_{2.5}$, particle aerodynamic diameter < 2.5 μm). NOx emissions have been increasing rapidly over the past decade (e.g., Richter *et al.*, 2002, Irie *et al.* 2016), and long-range nitrate transport is becoming increasingly important for regional nitrogen budget studies (e.g., Oita *et al.*, 2016, Itahashi *et al.*, 2016, 2017; Uno *et al.*, 2017a,b). A large proportion of nitrate exists in coarse mode (PM_c, particle aerodynamic diameter > 2.5 μm) due to interactions with sea salt and mineral dust. The formation of nitrate on dust aerosols has been clearly observed using
15   scanning electron microscopy (SEM), both in laboratory experiments and using field measurements (Li and Shao, 2009). Acid uptake of pollutants over sea salt and dust surfaces is important when evaluating coarse NO_3^-, as it modifies the chemical lifetime of nitric acid (including atmospheric loading and deposition). Continuous measurement of both fine- and coarse-mode aerosol compositions (including NO_3^-) is critical for achieving a complete understanding of the fate of air pollutants and changes in the Asian atmospheric environment (Li *et al*, 2012, Pan *et al*., 2017, Wang *et al*., 2017a).
20   Ground-based and airborne aerosol observations have been studied to determine the physics and chemistry of high-concentration events (e.g., Huebert *et al*., 2003; Jacob *et al*., 2003, KORUS-AQ, 2016), but the duration of these observational campaigns is typically less than 1 month, which is insufficient for studying seasonal variation. Monitoring projects conducted by the Acid Deposition Monitoring Network in East Asia (EANET; 2014) and Asian Dust and Aerosol Lidar Observation Network (AD-Net Lidar; Sugimoto *et al*., 2008), among others, have been accumulating observational
25   data for over 10 years, but detailed data on hourly aerosol compositions are rarely captured. Long-term aerosol observations (over at least 1 year), including of aerosol composition and with a high time resolution, are required because seasonal changes in Asian monsoons play an important role in the patterns and frequency of long-range pollutant transport; however, no such detailed observational studies have been undertaken to date.

We have made long-term synergetic observations of the behaviors of aerosols around the Chikushi Campus of Kyushu
30   University, located in the suburbs of Fukuoka City (33.52°N, 130.47°E), since October 2013 (Pan *et al*., 2015, 2106; Itahahsi *et al*., 2017; Uno *et al*., 2017a,b; Osada *et al*., 2016). We used a state-of-the-art aerosol observation instrument to measure both fine- and coarse-mode aerosols. In this study, we report seasonal variation in both fine- and coarse-mode atmospheric

aerosols based on long-term synergetic aerosol observations made at 1 h intervals in Fukuoka, Japan, from August 2014 to October 2015. During this period, several yellow sand and heavy pollutant transport episodes were observed. This paper reports on the major characteristics of anthropogenic aerosols and long-range dust transport, based on observations and chemical transport model (CTM) analysis. We focused on the seasonal variation in fine- and coarse-mode long-range nitrate

5 transport.

This report is structured as follows: Section 2 documents the observational dataset, Section 3 describes the CTM simulation in detail, Section 4 discusses temporal variations at observation sites and the model results, and Section 5 provides a summary and conclusions.

2 Observation

10 Observations were made on the rooftop (4F) of the Fukuoka Institute of Health and Environmental Science and the Chikushi Campus of Kyushu University, Fukuoka. The horizontal distance between these two sites is about 5 km. Both sites are located in a suburban area of Fukuoka. The anthropogenic activity was very limited at both sites, and the air quality showed similar patterns.

2.1 Aerosol Chemical Speciation Analyzer and NHx measurement

15 A continuous dichotomous Aerosol Chemical Speciation Analyzer (ACSA-12 Monitor; Kimoto Electric, Osaka, Japan), was utilized to measure PM_{10} (particulate matter < 10 μm in diameter) and $PM_{2.5}$ (particulate matter < 2.5 μm in diameter) with high temporal resolution (Kimoto et al., 2013). Particulate matter (PM) was collected on a tape filter made of Teflon (PTFE). Hourly observations were conducted to monitor SO_4^{2-}, NO_3^-, optical black carbon (BC), and water-soluble organic compounds (WSOC) at Fukuoka. The mass concentrations of PM were determined using the beta-ray absorption method.

20 The ACSA-12 measured NO_3^- and WSOC by an ultraviolet absorption-photometric method, and SO_4^{2-} by turbidimetry, after addition of $BaCl_2$ to form $BaSO_4$ and polyvinyl pyrrolidone as a stabilizer. Optical BC was measured using a near-infrared (NIR) light scattering method, and the observed data showed a good correlation with the IMPROVE protocol measurement (Hasegawa et al., 2004). The analytical period was within 2 h of sampling; therefore, the volatilization of particulate NH_4NO_3 after collection was regarded as minimal compared with the traditional filter-pack observation method. ACSA has

25 been tested previously (Osada et al., 2016) and used to identify aerosol chemical compositions at Fukuoka (Pan et al., 2016, Uno et al., 2017a, 2017b). It should be noted that ACSA-12 measures both fine- and coarse-mode aerosols simultaneously and is an important for mass budget studies and evaluation of CTMs.

The behaviors of NH_3 and NH_4^+ are also important because they are the counter-ions for SO_4^{2-} and NO_3^-. The concentrations of gaseous NH_3 and NH_4^+ in fine particles were measured with a semi-continuous microflow analytical system (Kimoto

30 Electric, MF-NH$_3$A, Osada et al., 2011). Two inlet lines were used to differentiate the total amounts of NHx and particulate NH_4^+ after gaseous NH_3 was removed using a phosphoric acid-coated denuder from the sample air stream. The cut-off

diameter of the inlet impactor was about 2 μm (which is smaller than the ACSA $PM_{2.5}$ cut-off). Secondary inorganic aerosols (SO_4^{2-}, NO_3^-, and NH_4^+; SNA) were fully observed using our synergetic monitoring system.

2.2 Denuder-filter pack method

5   During our observation period from August 2014 to October 2015, we conducted denuder-filter (D-F) pack measurements at the Chikushi Campus of Kyushu University, Fukuoka. An annular denuder–multi-stage filter sampling system was used for HNO_3 and size-segregated aerosol sampling. The sampling interval was 6−8 h for intensive observation and 1−2 days for regular observation. At the inlet, coarse-mode aerosols were removed by Nucleopore membrane filters (111114; Nomura Micro Science Co., Ltd., Atsugi, Japan [pore size = 8 μm]), and then gas-phase HNO_3 was collected with the annular

10   denuder (2000-30x242-3CSS; URG, Chapel Hill, NC, USA) coated with NaCl (Perrino *et al.*, 1990). Fine-mode aerosols were collected with a PTFE filter (J100A047A; ADVANTEC, Tokyo, Japan [pore size = 1 μm]), and a nylon filter (66509; Pall Co., Port Washington, NY, USA) captured volatized nitrates from the PTFE filter (Appel *et al.*, 1981; Vecchi *et al.*, 2009). The sample air flow rate was 16.7 L min^{-1} (1 atm, 25°C). Under these conditions, the aerodynamic diameter of the 50% cut-off for the Nucleopore filter was approximately 1.9 μm (John *et al.*, 1983). The samples were analyzed by ion

15   chromatography (IC). Fine-mode aerosols (< 1.9 μm in diameter) were underestimated by the D-F pack compared with the ACSA measurement, and coarse-mode aerosols (> 1.9 μm, with no upper limit) were overestimated by the D-F pack compared with the ACSA PM_c measurements (2.5−10 μm) due to a difference in cut-off diameter between the methods (Osada *et al.*, 2016). Details of the ACSA data comparison and validation were reported previously by Osada *et al.* (2016).

3 Numerical modeling

20   We used the 3-D Goddard Earth Observing System chemical transport model (GEOS-Chem) (ver. 09-02) (Bey *et al.*, 2001; Park *et al.*, 2004; Fairlie *et al.*, 2007, 2010). The model was run with the full GEOS-Chem NOx-Ox-VOC-HOx-CO chemistry option to simulate the formation of aerosols, including mineral dust, sea salt, and secondary inorganic aerosols (SO_4^{2-}, NO_3^-, NH_4^+). We also modeled the emission/transport of primary BC and organic carbon (OC). However, the detailed carbonaceous species and secondary organic aerosol (SOA) options in GEOS-Chem were not used in this study.

25   Dust in GEOS-Chem is classified according to four size bins (radii of 0.1−1.0, 1.0−1.8, 1.8−3.0, and 3.0−6.0 μm), based on Ginoux *et al.* (2004). The smallest size bin is further divided into 4 bins (radii 0.1−0.18, 0.18−0.3, 0.3−0.6, 0.6−1.0 μm) for optical properties and heterogeneous chemistry. This model uses the dust entrainment and deposition (DEAD) mobilization scheme from Zender *et al.* (2003), combined with the source function used in the Goddard Chemistry Aerosol Radiation and Transport (GOCART) model (Ginoux *et al.* 2001), as described by Fairlie *et al.* (2007). Several modifications to capture

30   seasonal changes in dust source function, the dust emission fraction within dust bins, and the change in wet scavenging efficiency that was inversely determined to fully capture Asian dust (Yumimoto *et al.*, 2017) were used in this study. The

general performance of our dust simulation was already reported by Yumimoto *et al.* (2017) and Uno *et al.* (2017a, b). Sea salt is distributed into two size bins (dry radii 0.01−0.5 and 0.5−8 μm). The sea salt emission scheme is based on the work of Jaeglé *et al.* (2011) and was well-validated by those authors. It includes the effects of sea-surface temperature (SST), as more sea salt is emitted in the summer.

5 In this study, the reactive uptake of HNO_3 and SO_2 on dust (limited by dust alkalinity), and the uptake of gas-phase H_2SO_4 (limited by competition with other aerosol surfaces) (Fairlie *et al.*, 2010) were used. Dust-nitrate (mainly $Ca(NO_3)_2$) was simulated based on the heterogeneous reaction between dust and nitric acid, as follows:

$$CaCO_3 + 2HNO_3 \rightarrow Ca(NO_3)_2 + H_2O + CO_2 \quad (R1)$$
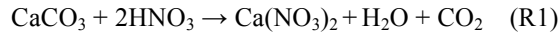
As described by Fairlie *et al.* (2010), the first-order reactive uptake rate constant (k) is calculated according to the uptake coefficient (γ) and surface area density of dust particles (A) using the following equation, suggested by Jacob (2000):

$$-\frac{dC}{dt} = \left[\frac{r}{D_g} + \frac{4}{c\,\gamma}\right]^{-1} A\,C = k\,C \qquad (1)$$

where C is the concentration of gas uptake (e.g., HNO_3), r is the aerosol particle radius, D_g is the molecular diffusion
15 coefficient, and c is the mean molecular speed. The uptake coefficient depends on the ambient relative humidity (RH), and we used the RH-dependent function in Fig. 1 of Fairlie *et al.* (2010). More details on dust-nitrate formation from a heterogeneous reaction can be found in Fairlie *et al.* (2010). A similar heterogeneous reaction to that described by Eq. (1) for sea salt was also included in our calculation.

The model used the assimilated meteorological fields from the GEOS of the NASA Global Modeling and Assimilation
20 Office (GMAO). The model has a horizontal resolution of 2° × 2.5° for global runs, and 0.5° × 0.667° for Asian one-way nesting runs (11°S−55°N, 70−150°E,), both having 47 vertical levels from the surface to 0.01 hPa. The lowest model layer thickness was approximately 130 m. We used anthropogenic emissions data from the Emission Database for Global Atmospheric Research (EDGAR, ver. 3) (Olivier and Berdowski, 2001) for the global domain and the Regional Emission Inventory in Asia (REAS, ver. 2.1) for the Asian domain, as reported by Kurokawa *et al.* (2013). The REAS NH_3 emissions
25 were modified to include seasonal variations in Asia based on Huang *et al.* (2012), and further changes in winter emissions recommended by Xu *et al* (2015). Volcanic SO_2 emission is based on the database of the Japan Meteorological Agency (http://www.data.jma.go.jp/svd/vois/data/tokyo/volcano.html). The model simulation was conducted from the beginning of December 2013 to the end of October 2015, and results from the first 8 months were used to train the model. Other basic numerical settings were as reported in Uno *et al.* (2017a, b).

30 To investigate whether domestic or transboundary air pollution is dominant in Japan, we also performed a sensitivity simulation. Because the quantity of emissions from China was larger than that from Japan, to avoid large nonlinearities in the atmospheric concentration response to emissions variation (e.g., Itahashi *et al.*, 2015), a sensitivity simulation was

designed to include a 20% reduction in all emissions from Japan (defined as JOFF20%). Based on differences between the baseline simulation (CNTL) and the JOFF20% simulation, the domestic contribution from Japan (JOFF) was estimated using a multiple of 5 for differences in CNTL and JOFF20% experiments. We also made a volcanic SO_2 sensitivity simulation without volcanic SO_2 emissions (VOFF) because the SO_2 to SO_4^{2-} formation can be assumed to be linear.

5   Based on the analysis of PM concentrations, $PM_{2.5}$ and PM_{10} were calculated by summing the individual aerosol (SO_4^{2-}, NO_3^-, NH_4^+, BC and OC), dust, and sea salt components of the model. Hereafter, we denote modeled ammonium nitrate (i.e., NH_4NO_3) as A-NO_3^-, dust-nitrate as D-NO_3^-, sea salt nitrate as SS-NO_3^-, and their sum as simply NO_3^- (= A- + D- + SS-NO_3^-).

4 Results and Discussion

10   **4.1 Meteorological variation and sea salt**

Figure 1 shows the location of the observation sites, Fukuoka and the Mt. Sakurajima volcano, and the anthropogenic SO_2 emission distribution used in the model calculation. Figure 2 shows (a) the daily mean and maximum wind speed, (b) the daily mean temperature, RH, and precipitation in Fukuoka, as observed by the Japan Meteorological Agency, and (c) the observed coarse-mode Na^+ by D-F, and GEOS-Chem-simulated coarse-mode sea salt. The GEOS-Chem-simulated coarse

15 mode sea-salt concentration was converted to the Na concentration based on the salinity and Na mass ratio of sea water (Keene *et al*., 1986).

Japanese weather is controlled by changes in Asian monsoons. Under summer monsoon conditions (covered by S-SE wind from the hot and moist air mass of the Pacific High), air temperature and RH are at their maximum, while during the winter monsoon (N-NW continental cold air outflow), low temperatures and less precipitation are observed in Fukuoka. Maximum

20 wind speeds in excess of 10 m s^{-1} in summer−fall show the effects of typhoons (Fig. 2a). The precipitation difference between August 2014 and August 2015 is important for examining differences in the NH_3 concentration (August 2014 had more rainfall than August 2015), and we will discuss this in Section 4.3.4.

The time variation of modeled coarse-mode Na^+ generally agreed well with observations, except during typhoon events. There were five typhoons between July and September 2015, and the modeled cNa^+ was very high compared with

25 observations. This indicated that the sea salt emission scheme for very strong wind conditions was overestimated. We also observed high precipitation during the typhoon events. Another important difference is that the typhoon in 2014 occurred in the fall (September−October), after the SST had cooled, while in 2015 it occurred in the summer (July−August) when the SST was warm and more sea salt was emitted.

4.2 Daily variation and validation of modelling reproducibility

30 The monthly variation depends on the how well the model can reproduce the daily variation in the long-range transport from continental Asia to Japan, as well as sporadic dust transport. In this section, we analyzed this short-term daily variation and

sporadic dust phenomena, and validated the model performance statistically. The monthly (seasonal) variation of aerosols is discussed in Section 4.3.

Figure 3 shows the temporal variation in (a) $PM_{2.5}$, (b) PM_{10}, (c) optical BC, (d) fine SO_4^{2-}, (e) fine NO_3^-, and (f) coarse NO_3^- observations at Fukuoka. The ACSA observations are indicated in blue; D-F pack observations are indicated by the red line (spike-like high peaks during the dust event are due to large particles >10 µm, which is the cut-off in ACSA sampling). The figures also include the corresponding model values from the model control experiment (CNTL; gray shading). Both the observation and model results are shown as daily averaged values. The modeled cNO_3^- in (f) is the sum of dust- and sea salt-nitrates, and yellow shading indicates the modeled dust-coarse NO_3^- (D-cNO_3^-) fraction. **Table 1** shows the statistical analysis used to determine model reproducibility (results of linear regression are shown within the figure).

The observed $PM_{2.5}$ clearly exhibited frequent spike-like peaks from winter to early spring, but the frequency decreased after April according to the frequency of "polluted" cold air outbreaks from the Asian continent. The modeled $PM_{2.5}$ reproduced most of the observed variation. The modeled $PM_{2.5}$ had a high correlation ($PM_{2.5\_model} = 0.58$ ($PM_{2.5\_obs}$) + 1.16 µg m^{-3}, $R = 0.72$) but was underestimated (normalized mean balance (NMB) = –35.7%) because the observation data included aerosol compositions that were not incorporated into the model (e.g., SOAs, many trace metals, and others).

The observed PM_{10} included coarse aerosols (e.g., dust and sea salt), and peaks corresponded to major dust events. Symbols A−G in Fig. 3b are the major dust events that occurred during our observation period (Uno *et al*., 2017b). The time variation of modeled PM_{10} was in good agreement with observations, but was consistently underestimated (NMB = –31.3%) for the same reasons as for $PM_{2.5}$ (i.e., more coarse aerosols were included in the observed data than in the model) and showed some uncertainty for large dust concentrations (Uno *et al*., 2017b).

The modeled BC was systematically underestimated from July to December, but was at reasonable levels during the winter. The modeled BC also shows a similar underestimation (NMB = –32%), although R had a smaller value (0.34) than for $PM_{2.5}$. One possible explanation is the underestimation of Japanese domestic BC emissions (e.g., Itahashi *et al*., 2017).

We can see very good agreement for fine SO_4^{2-}, with NMB = –1.5% and R = 0.68. This indicated that the modeled fSO_4^{2-} reproduced most of the observed variation quite well. Figure 3(d) shows intermittently high SO_4^{2-} concentrations. The high SO_4^{2-} levels in the winter depended on the frequency of LRT from the Asian continent based on the synoptic weather change that occurred once or twice/week, while high SO_4^{2-} levels are usually observed in summer (see also Fig. 4b). This is related to the meteorological conditions, i.e., the high RH in summer. Figure 3d shows high SO_4^{2-} levels from the end of July until early August 2015 (designated SVolc in the figure); this was used to demonstrate that the period of volcano impact is important for SO_4^{2-} levels. These high SO_4^{2-} concentrations were due to Japanese domestic emissions and volcanic SO_2

emissions. Because volcanic emissions are a natural phenomenon, and the day-by-day changes are difficult to predict, the modeled SO_4^{2-} level during SVolc misses the observed peak SO_4^{2-} (see the appendix for a more detailed analysis).

For fNO_3^-, the daily maximum reached 6−9 µg m^{-3} and was sometimes higher than the fSO_4^{2-}, with the same timing regarding the peaks as for SO_4^{2-}. This indicated that fNO_3^- was also controlled by LRT from the Asian continent (as discussed by Itahashi *et al*., 2017 and Uno *et al*., 2017b); NMB = −8.5% and R = 0.68. The correlation is the same as for fSO_4^{2-}, but has a larger NMB than fSO_4^{2-}. Coarse NO_3^- had a distinct peak value during dust events A−G (D-F cNO_3^- levels are higher than ACSA cNO_3^- levels due to different upper cut-off limits). The modeled cNO_3^- levels were higher (see Fig. 3c and 4g) during the fall (October to November) because of sea-salt NO_3^- and during the dust season (typically from February to June). Coarse NO_3^- takes a larger NMB compared with fine NO_3^- and is underestimated. This can be understood because cNO_3^- depends on the prediction accuracy of dust and sea-salt.

As shown in Fig. 3, a regression slope that is less than 1 could be a natural phenomenon owing to representation issues regarding the model and observations. The GEOS-Chem model result is an average value over a 0.5° × 0.667° grid, while the observation is conducted over a station. This is another reason why the simulated model results tend to be underestimated at the high end and overestimated at the low end, which results in a slope less than 1.

For all of the components shown in Table 1, the mean fractional bias (MFB) ranges between -51.0% and -8.96%, and the mean fractional error (MFE) ranges between 47.99% and 85.75%. Except for fNO_3^-, these results satisfied the model performance criteria (MFB < ±60% and MFE < ±75 %) proposed by Boylan and Russell (2006). Wang *et al*.(2017b) also reported a similar score for fNO_3^- for different chemical transport models (CMAQ and NAQPMS) and this may be a limitation of current CTMs.

4.3 Monthly variation in aerosol compositions

Figure 4 shows the monthly average (a) $PM_{2.5}$, (b) fine- and coarse-mode SO_4^{2-}, (c) fine and coarse NH_4^+, (d) NH_3 gas, (e) HNO_3, (f) total NO_3^-, (g) coarse NO_3^-, and (h) fine NO_3^- levels. The box-whisker plots show the observed fine aerosol levels (10th, 25th, 50th, 75th and 90th percentile values are marked). The observed average monthly coarse-mode aerosols are shown by the red dashed line. The modeled average monthly fine aerosol concentration for the CNTL is depicted by the straight black line, and by the black dashed line for the JOFF.

4.3.1 Fine-mode SO_4^{2-} and NH_4^+

The modeled SO_4^{2-} results explained the observed temporal variation and corresponded to approximately 37% of the modeled $PM_{2.5}$ concentration (daily base regression: $SO_4^{2-}{}_{model} = 0.82(SO_4^{2-}{}_{obs}) + 0.76$ µg m^{-3}, $R = 0.68$; $SO_4^{2-}{}_{model} = 0.37(PM_{2.5\_model}) + 0.40$ µg m^{-3}, $R = 0.81$). The high correlation suggests that the variations in $PM_{2.5}$ were mainly driven by
5   fSO_4^{2-}, as a main component of $PM_{2.5}$ for both the observations and the model. The model underestimated fSO_4^{2-} levels from December to January. Similar underestimation was observed in other CTM applications (Wang *et al.*, 2017b; Itahashi *et al.*, 2017), and in the observations of He *et al.* (2014).

Based on Fig. 4, SO_4^{2-} and NH_4^+ levels are reasonably well predicted by the model. The JOFF sensitivity analysis showed that the contribution from Japanese emissions was small and the majority of SO_4^{2-} came from LRT from outside of Japan
10 (annual mean Japanese domestic contribution = 15%). For NH_4^+, we found that the LRT contribution was large until April, after which the Japanese contribution increased as NH_3 emissions increased (annual mean Japanese domestic contribution = 27%).

Coarse mode SO_4^{2-} was about 0.1−0.2 of fine SO_4^{2-} (monthly average relationship: $cSO_4^{2-} = 0.185 \, fSO_4^{2-} - 0.052$ µg m^{-3}, $R = 0.66$). The coarse SO_4^{2-} contribution cannot be ignored in winter. Modeled cSO_4^{2-} levels were very small compared to
15 observed levels and are not shown in the figure.

4.3.2 Fine-mode NO_3^-

The modeled fNO_3^- reproduced the major monthly variation seen in the observed levels. fNO_3^- levels are higher during the winter and lower during the summer, exhibiting clear seasonal changes. The winter (DJF) fNO_3^- average was 2.62 ± 1.64 µg
20 m^{-3}. The JOFF sensitivity analysis also confirmed that the majority of fNO_3^- can be considered due to LRT from outside Japan during the winter. In the summer, fNO_3^- is minimal because the NH_4NO_3 equilibrium between NH_3 and HNO_3 shifts to the gaseous phase under warm conditions. This phase shift is a function of temperature and RH, and it moves to an aerosol phase at cold temperatures. The monthly average fNO_3^- from June to September was 0.68 ± 0.34 µg m^{-3}. It should be noted that NO_3^- measurement by ACSA was finished within 2 h of PTFE sampling, so any artifact due to the volatilization of NO_3^-
25 from the Teflon filter surface was small (e.g., Osada *et al.*, 2016). As described in section 2, D-F measurement used the nylon backup filter to catch the volatilized HNO_3 from the Teflon filter surface. Thus, both ACSA fNO_3^- and D-F fNO_3^- measurements showed consistent concentrations during the summer (average = 0.43−0.68 µg m^{-3}; see Fig. 3e.) From mid-May to October, the Japanese contribution becomes dominant (annual mean Japanese domestic contribution = 53%).

4.3.3 Coarse-mode NO_3^-

Figure 4(g) shows the clear seasonal cycle of modeled cNO_3^-. The modeled results showed that dust-nitrate concentrations increased during dust episodes. Modeled sea salt-nitrate was consistently in the order of 0.5−1.0 μg m^{-3} as the baseline cNO_3^-, and it was dominant, except during the dust season (showing good agreement with observed values).

Table 2 summarizes the comparison of cNO_3^- levels. Except for January to June, sea salt-NO_3^- was dominant within cNO_3^-, and the model results were in good agreement with actual observations. From January to June, the ratio of D-cNO_3^- to SS-$cNO_3^- \approx$ 1:1 and the modeled total cNO_3^- corresponded to two-thirds of the observed total cNO_3- (annual average ratio of D-cNO_3^- to SS-$cNO_3^- \approx$ 1 : 2.4). From January−June 2015, we observed several dust events (designated A−G). Uno *et al*. (2017b) described the typical onset of dust events B and C, and pointed out underestimation of the modeled cNO_3^- during these cold dust cases. In this paper, we examine dust event G as a case study of warm weather dust acid uptake validation.

Figure 5 shows the daily changes in dust (colored region) and total D-cNO_3^- (contoured area) horizontal distributions from (a) June 12 to (b) June 13, and the Hybrid Single Particle Lagrangian Integrated Trajectory (HYSPLIT) model back trajectory starting from Fukuoka. It also shows a comparison of modeled and observed (c) fine- and (d) coarse-mode NO_3^-. The dust transport path was very similar to those of dust events B and C, as described by Uno *et al*. (2017b). For dust events B and C (see Fig. 3f), modeled cNO_3^- was underestimated, but for dust event G, modeled cNO_3^- levels were in good agreement with observed levels. Modeled results show that D-cNO_3^- mainly formed over the Yellow Sea and the East China Sea. This indicates that the underestimation of dust-NO_3^- over the winter was independent of the dust acid uptake scheme. These results indicate the importance of further studies on the mechanism of cNO_3^- formation.

4.3.4 Monthly variation in total NO_3 and NH_x

Figure 6 shows the observed monthly variation in (a) fNH_4^+, cNH_4^+, and NH_3, (b) fNO_3^-, cNO_3^-, and HNO_3, and (c) the relative mass fraction of NO_3^- and HNO_3. From this figure, fNO_3^- clearly showed the highest concentration in winter, while HNO_3 increased in summer (HNO_3 accounted for 30−40% of total NO_3^-); this was due to the change in thermal equilibrium between gases and particles. Notably, cNO_3^- was always higher than fNO_3^- (cNO_3^- made up 27−55% of the total NO_3^-, and it exceeded 45% in winter). We observed 0.5−1.0 μg m^{-3} (0.2−0.4 ppb) of HNO_3 even in winter.

The observations showed that fine NH_4^+ is higher throughout the year, and the NH_3 gas level exceeded 1 μg/m^3 (0.4 ppb), even in winter. This high NH_3 concentration may be influenced by local agriculture and poultry farming 5−10 km south of the observation site. The high NH_3 concentration (see Fig. 4d) in August 2015 (3–4 times higher than in August 2014) might be due to differences in the high temperature (the monthly mean was 28.4°C, which was 1.7°C higher than in 2014) and less precipitation (month total was 186 mm, which was 228 mm smaller than in 2014). Roelle *et al*. (2002) indicated that the NH_3 emission from soil increased exponentially as soil temperature increased, and more soil water due to precipitation fills the pores in the soil matrix and hinders the diffusion of NH_3 from the soil to the air. Their results suggested that our observed meteorological conditions in each year can explain the NH_3 concentration variation. The annual average cNH_4^+/total NH_x

ratio was 10%, but it increased to 15% (JFM average). This indicates that the cNH_4^+ counterpart in winter is important for understanding cNO_3^- and cSO_4^{2-}.

The model results underestimated NH_3 (Fig. 4d) and overestimated HNO_3 (Fig. 4e); however, the modeled total NO_3^-, fNO_3^- and fNH_4^+ levels were in good agreement with the observed values (compared with Fig. 4h, 4g, and 4c, respectively). The

5   NH_3 emissions inventory is at 25 km resolution, and cannot reflect the impact of local agriculture and poultry farming, which has large uncertainty; this results in the underestimation of NH_3 emissions in our study. On the other hand, most of the cNO_3^- formation occurred before arrival in Japan (it occurred mainly over the ocean), and was also not very sensitive to local NH_3 emissions.

The present model does not include the formation scheme of cNH_4^+. The counterparts of cNH_4^+ can be cNO_3^- and cSO_4^{2-},

10   and this is one of the reasons for cNO_3^- underestimation by the model. It is important to describe the possible reasons for this underestimation to conduct a detailed N budget study, because the cNO_3^- fraction is very large. Another interesting question is whether the modeled acid-uptake scheme can explain the observed cNO_3^- levels in dust and sea salt. We used statistical analysis to investigate this.

4.4 Statistical analysis of coarse-mode NO_3^-

15   Major sources of cNO_3^- include dust, sea salt and other sources, represented as cNH_4^+. We conducted MRA to analyze cNO_3^-. We included cNa^+, $nss\text{-}cCa^{2+}$ and cNH_4^+ as independent variables to describe the observed cNO_3^- (cSO_4^{2-} was excluded from the MRA due to its strong colinearity with cNH_4^+). One important point is that the observation site is surrounded by school grounds and a large city park, providing background local dust. We found that the median value of $nss\text{-}cCa^{2+}$ during the non-dust season was 0.25 µg m^{-3}, and the residence time of local dust coming to the observation site for producing cNO_3^- was

20   short (< 1 h). We excluded observations less than $nss\text{-}cCa^{2+} < 0.25$ µg m^{-3} from the MRA.

The result of the MRA (n = 160, $nss\text{-}cCa > 0.25$ µg m^{-3}) was

$$cNO_3^- = 0.51\ cNa^+ + 1.58\ nss\text{-}cCa^{2+} + 2.2\ cNH_4^+ + 0.19\ \text{µg m}^{-3}\ (R^2 = 0.74,\ p<0.001)$$

where the term on the right can be considered to represent SS-cNO_3^-, D-cNO_3^-, and cNO_3^- accompanied by cNH_4^+, respectively.

25   **Figure** 7 shows the contribution of (a) MRA D-cNO_3^- = 1.58 × $nss\text{-}cCa^{2+}$ for $nss\text{-}cCa^{2+} > 0.25$ µg m^{-3}, and (b) MRA SS-cNO_3^- = 0.51 × cNa^+. The figure also includes the GEOS-Chem modeled results (averaged over the same time period as for the D-F measurements). MRA D-cNO_3^- showed good agreement with modeled D-cNO_3^- levels (except for intensive dust events B and C), and this indicates that the dust acid-uptake scheme explains the observed dust-nitrate formation (underestimation for B and C also comes from the underestimation of modeled dust concentrations). As previously pointed

30   out, modeled SS-cNO_3^- was over predicted during the summer typhoon period; aside from these periods, good agreement was found with sea salt cNO_3 (Fig. 7b).

Figure 8 shows the monthly averaged MRA results and clearly explains the observed seasonal variation. **Table** 2 summarizes each term and shows the comparison with CTM. The average annual contribution of each term was 40% for SS-

cNO$_3^-$, 20% for D-cNO$_3^-$ and 40% for cNH$_4^+$ term. The D-cNO$_3^-$ value was high during the dust season, and the sea salt component made the largest contribution throughout the year. The cNH$_4^+$ term made a large contribution during the winter, and one possible reason for this is the condensation/coagulation of small NH$_4$NO$_3$ and (NH$_4$)$_2$SO$_4$ particles onto large particles (e.g., sea salt and dust). The annual average D-cNO$_3^-$ to SS-cNO$_3^-$ ratio in MRA was 1 : 2, which is close to the modeled ratio (1 : 2.4), as shown in Table 2.

Our results suggest that inclusion of aerosol microphysical processes (such as condensation and coagulation of the fine anthropogenic aerosols NO$_3^-$ and SO$_4^{2-}$ onto the coarse particles) is important for exploring the observed cNO$_3^-$ concentrations. A CTM incorporating advanced particle microphysics (APM) is one potential option (Yu and Luo, 2009). Such a modeling approach, incorporating interactions with mineral dust and sea salt, has not yet been fully explored in East Asia and is a future research direction.

5 Conclusions

Long-term synergetic fine- and coarse-mode aerosol observations were analyzed at 1 h intervals in Fukuoka, Japan, from August 2014 to October 2015. A GEOS-Chem chemical transport model including dust and sea salt acid uptake processes was used for detailed analysis of observation data to understand the effects of LRT from the Asian continent. The findings from this study can be summarized as follows:

1) Continuous measurement of SO$_4^{2-}$, NO$_3^-$, and optical BC with the ACSA-12 monitor, and of NH$_4^+$ and NH$_3$ with a semi-continuous microflow analytical system (MF-NH3A) in addition to D-F pack/IC analysis, established a long-term synergetic fine- and coarse-mode aerosol database in Fukuoka, Japan.

2) During the observation period, several Asian dust and long-range anthropogenic aerosol transport events were observed, and a numerical model generally explained the observed temporal variation. A dust concentration by dust emission inversion scheme effectively reproduced the major dust onset.

3) Numerical results explained the seasonal changes in fine aerosols (SO$_4^{2-}$, NO$_3^-$, and NH$_4^+$), and the impact of LRT, and a sensitivity analysis excluding Japanese domestic emissions revealed the LRT fraction (85% for fSO$_4^{2-}$, 47% for fNO$_3^-$ and 73% for fNH$_4^+$).

4) Observational data for HNO$_3$, fNO$_3^-$, and cNO$_3^-$ confirmed that there was a large amount of coarse NO$_3^-$ comprising 40−55% of total nitrate during the winter; meanwhile, HNO$_3$ gas made up 40% of total nitrate in summer, and fine NO$_3^-$ peaked during the winter. A numerical model reproduced the seasonal variation in fine NO$_3^-$. For coarse NO$_3^-$, modeled cNO$_3^-$ was in good agreement with observations between July and November (mainly coming from sea salt-NO$_3^-$).

5) Large-scale dust-nitrate outflow from China to Fukuoka was confirmed in all dust events. During the winter, modeled coarse NO$_3^-$ was underestimated compared to the observed levels.

6) The coarse NO_3^- underestimation was examined statistically using MRA. We included cNa^+, nss-cCa^{2+} and cNH_4^+ as independent variables to describe the observed cNO_3^-; these terms can be considered to represent SS-cNO_3^-, D-cNO_3^-, and cNO_3^- accompanied by cNH_4^+, respectively. The MRA results showed a high correlation, $R^2 = 0.74$, and clearly explained the observed seasonal changes. The annual average contributions of the component were 40% (SS-cNO_3^-), 20% (D-cNO_3^-), and 40% (cNH_4^+ term). The D-cNO_3^- component had the largest value during the dust season, and the sea salt component made a large contribution throughout the year. cNH_4^+ made a large contribution during the winter; one possible reason for this was the condensation/coagulation of small NH_4NO_3 and $(NH_4)_2SO_4$ particles onto large particles (e.g., dust and sea salt).

The present model did not include aerosol microphysical processes (such as condensation and coagulation between fine anthropogenic aerosols, such as NO_3^- and SO_4^{2-}, and coarse particles), but our results suggest that aerosol microphysical processes are important for studying observed cNO_3^- formation, especially in winter.

Data availability. To request the observation data used in this study for scientific research purposes, please contact Itsushi Uno at Kyushu University via email (uno@riam.kyushu-u.ac.jp). The model simulations were based on GEOS Chem, open-source and publicly available software. The model and related software can be downloaded from http://acmg.seas.harvard.edu/geos/ by registered users.

Author contributions. Itsushi Uno designed the synergetic observations at Chikushi Campus of Kyushu University, Japan. Shigekazu Yamamoto and Kazuo Osada carried out the ground-based ACSA and NHx-monitor observations, respectively, at Fukuoka. Kazuo Osada conducted air sampling and chemical analysis of D-F pack samples during the observation period at Fukuoka. Yugo Kanaya and Xaiole Pan conducted the CO observations at Fukuoka. T. Duncan Fairlie provided the GEOS Chem modeling system. Itsushi Uno, Keiya Yumimoto, Syuichi Itahashi and Zhe Wang performed the model simulations and analysis, and prepared the paper with contributions from all coauthors.

Competing interests. The authors declare that they have no conflicts of interest.

Acknowledgments. This work was supported by the Ministry of Education, Culture, Sports, Science and Technology (MEXT), the Japan Society for the Promotion of Science (JSPS) and the Grants-in-Aid for Scientific Research (KAKENHI) program (Grant JP25220101). The authors would like to thank the developers of the GEOS reanalysis product. This work was partly funded by a collaborative research program through the Research Institute for Applied Mechanics at Kyushu University (no. 26AO-2, 27AO-6, 28AO-2). We thank Yusuke Kamiguchi at Nagoya University for the D-F pack sampling and chemical analysis and Shohei Kuwahara at Kyushu University for the D-F pack sampling.

References

Bey, I., J. Jacob, R. M. Yantosca, A. Logan, B. D. Field, A. M. Fiore, Q. Li, H. Y. Liu, J. Mickley, and M. G. Schultz: Global modeling of tropospheric chemistry with assimilated meteorology: Model description and evaluation, *J. Geophys. Res.*, **106**, 73–95, 2001.

Boylan, J.W., Russell, A.G.: PM and light extinction model performance metrics, goals, and criteria for three-dimensional air quality models. *Atmos. Environ.* **40**, 4946-4959, 2006.

EANET: EANET and Clean Air for Sustainable Development. The Third Report for Policy Makers (RPM3). Acid Deposition Monitoring Network in East Asia (EANET). Pathumthani, Thailand, 2014.

Fairlie, T.D., Jacob, D.J., Park, R.J.: The impact of transpacific transport of mineral dust in the United States, *Atmos. Environ.,* **41**, 1251–1266, 2007.

Fairlie, T.D., Jacob, D.J., Dibb, J.E., Alexander, B., Avery, M.A., A. van Donkelaar, Zhang, L.: Impact of mineral dust on nitrate, sulfate, and ozone in transpacific Asian pollution plumes, *Atmos. Chem. Phys.*, **10**, 3999–4012, 2010.

Genfa, Z., Dasgupta, P.K., Dong, S.: Measurement of atmospheric ammonia. *Environ. Sci. Technol.*, **23**, 1467–1474, 1989.

Ginoux, P., Chin, M., Tegen, I., et al.: Sources and distributions of dust aerosols simulated with the GOCART model, *J. Geophys. Res.*, **106**(D17), 20255–20274, 2001.

Ginoux, P., Prospero, J. M., Torres, O., and Chin, M.: Long-term simulation of global dust distribution with the GOCART model: correlation with North Atlantic Oscillation, Environ. *Modell. Softw.*, **19**, 113–128, 2004.

Hasegawa, S., Wakamatsu, S., and Tanabe, K.: Parallel measurement test of black carbon monitors, *Proceeding of 21th Symposium on Aerosol Science and Technology*, Japan Association of Aerosol Science and Technology, p. 7, 2004 (in Japanese).

He, H., Wang, Y., Ma, Q., Ma, J., Chu, B., Ji, D., Tang, G., Liu C., Zhang, H., Ho, J.: Mineral dust and NOx promote the conversion of SO$_2$ to sulfate in heavy pollution days, *Scientific Reports*, **4**, 4172, doi:10.1038/srep04172, 2014.

Huang, X., Song, Y., Li, M., Li, J., Cai, X., Zhu, T., Hu, M., Zhang, H.: A high-resolution ammonia emission inventory in China, *Global Biogeochem. Cycles,* **26**, GB1030, doi:10.1029/2011GB004161, 2012.

Huebert, B. J., Bates, T., Russell, P. B., Shi, G., Kim, Y. J., Kawamura, K., Carmichael, G., and Nakajima, T.: An overview of ACE-Asia: Strategies for quantifying the relationships between Asian aerosols and their climatic impacts, *J. Geophys. Res.*, **108(**D23), 8633, doi:10.1029/2003JD003550, 2003.

Irie, H., Muto, T., Itahashi, S., Kurokwa, J. and Uno, I.: Turnaround of tropospheric nitrogen dioxide pollution trends in China, Japan, and South Korea, *SOLA*, **12**, 170−174, doi:10.2151/sola.2016-035, 2016.

Itahashi, S., Hayami, H., Uno, I.: Comprehensive study of emission source contributions for tropospheric ozone formation over East Asia, J. *of Geophys. Res,* **120**, 331-358, 2015.

Itahashi, S. H. Hayami, I. Uno, X.L. Pan, M. Uematsu: Importance of coarse-mode nitrate produced via sea salt as atmospheric input to east Asian oceans. *Geophysical Research Letters*, **43**, doi:10.1002/2016GL068722, 2016.

Itahashi, S., Uno, I., Osada, K., Kamiguchi, Y., Yamamoto, S., Tamura, K., Wang, Z., Kurosaki, Y., Kanaya, Y.: Nitrate transboundary heavy pollution over East Asia in winter, *Atmos. Chem. Phys.*, **17**, 3823-3843, 2017.

5   Jacob, D.: Heterogeneous chemistry and tropospheric ozone, *Atmos. Environ.*, **34**, 2131–2159, 2000.

Jacob, D., J. Crawford, M. Kleb, V. Conners, R. Bendura, J. Raper, G. Sachse, J. Gille, and L. Emmons: Transport and chemical evolution over the Pacific (TRACE-P) mission: Design, execution, and overview of first results, *J. Geophys. Res.*, **108**(D20), 8781, doi:10.1029/2002JD003276, 2003.

Jaeglé, L., P.K. Quinn, T. Bates, B. Alexander, and J.-T. Lin (2011). Global distribution of sea salt aerosols: New constraints
10   from in situ and remote sensing observations, *Atmos. Chem. Phys.*, **11**, 3137-3157, doi:10.5194/acp-11-3137-2011.

Keene. W.C., A.A.P. Pszenny, J.N. Galloway, and M.E. Hawley: Sea-salt corrections and interpretation of constituent ratios in marine precipitation, *J. Geophysical Research*, **91**, 6646–6658, 1986.

Kimoto, H., Ueda, A., Tsujimoto, K., Mitani, Y., Toyasaki, Y. and Kimoto, T.: Development of continuous dichotomous aerosol chemical speciation analyzer, *Clean Technol.*, **23**, 49–52, 2013 (in Japanese).

15   KORUS-AQ: https://espo.nasa.gov/home/korus-aq/content/KORUS-AQ.

Kurokawa, J., Ohara, T., Morikawa, T., Hanayama, S., Janssens-Maenhout., G, Fukui, T., Kawashima, K., Akimoto, H.: Emissions of air pollutants and greenhouse gases over Asian regions during 2000–2008: Regional Emission inventory in ASia (REAS) version 2, *Atmos. Chem. Phys.*, **13**, 11019–11058, 2013.

Lawrence, M.G., Lelieveld, J.: Atmospheric pollutant outflow from southern Asia: a review. *Atmospheric Chemistry and*
20   *Physics,* **10**, 11017–11096, 2010.

Li, J., Du, H., Wang, Z., Sun, Y., Yang, W., Li, J., Tang, X., Fu, P.: Rapid formation of a severe regional winter haze episode over a mega-city cluster on the North China Plain. *Environmental Pollution,* **223**, 605-615, 2017.

Li, W.J., Shao, L.Y.: Observation of nitrate coatings on atmospheric mineral dust particles. *Atmospheric Chemistry and Physics,* **9**, 1863-1871, 2009.

25   Li, J., Wang, Z.F., Zhuang, G., Luo, G., Sun, Y., Wang, Q.: Mixing of Asian mineral dust with anthropogenic pollutants over East Asia: a model case study of a super-dust storm in March 2010. *Atmospheric Chemistry and Physics,* **12**, 7591-7607, 2012.

Ohara, T., *et al*.: REAS: Asian emission inventory for anthropogenic emission sources during the period 1980– 2020, *Atmos. Chem. Phys*., **7**, 4419–4444, 2007.

30   Oita, A., Malik, A., Kanemoto, K., Geschke, A., Nishijima, S., and Lenzen, M.: Substantial nitrogen pollution embedded in international trade. *Nat. Geosci.* **9**, 111–115, 2016.

Olivier, J.G.J. and J.J.M. Berdowski, *Global emissions sources and sinks*. In: Berdowski, J., Guicherit, R. and B.J. Heij (eds.) *The Climate System*, 33-78. A. A. Balkema Publishers/Swets & Zeitlinger Publishers, Lisse, The Netherlands, 2001.

Osada, K., Ueda, S., Egashira, T., Takami, A., Kaneyasu, N.: Measurement of gaseous NH3 and particulate NH4+ in the atmosphere by fluorescent detection after continuous air-water droplet sampling, *Aerosol and Air Quality Research,* **11**, 170–178, 2011.

5   Osada, K., T. Kamikuchi, S. Yamamoto, S. Kuwahara, X. Pan, Y. Hara, I. Uno: Comparison of ionic concentrations on size-segregated atmospheric aerosol particle based on a denuer-filter method and a Continuous Dichotomous Aerosol Chemical Speciation Analyzer (ACA-12), *Earozoru Kenkyu*, **31**, 203–209, 2016 (in Japanese with English abstract).

Pan, X., Uno, I., Wang, Z., Nishizawa, T., Sugimoto, N., Yamamoto, S., Kobayashi, H., Sun, Y., Fu, P., Tang, X., Wang, Z.: Real-time observational evidence of changing Asian dust morphology with the mixing of heavy anthropogenic pollution. *Scientific Reports* **7**, 335, DOI:10.1038/s41598-017-00444-w, 2017.

10   Pan, X., Uno, I., Hara, Y., Kuribayashi, M., Kobayashi, H., Sugimoto, N., Yamamoto, S., Shimohara, T., Wang, Z.: Observation of the simultaneous transport of Asian mineral dust aerosols with anthropogenic pollutants using a POPC during a long-lasting dust event in late spring 2014. *Geophysical Research Letters* **42**, 1593-1598, 2015.

Park, R. J., Jacob, D. J., Field, B. D., Yantosca, R. M., Chin, M.: Natural and transboundary pollution influences on sulphate-nitrate-ammonium aerosols in the United States: implications for policy, *J. Geophys. Res.*, **109**, D15204, doi:10.1029/2003JD004473, 2000.

15   Perrino, C., Santis, F. D., Febo, A.: Criteria for the Choice of a Denuder Sampling Technique Devoted to the Measurement of Atmospheric Nitrous and Nitric Acids, *Atmos. Environ.,* **24**, 617-626, 1990.

Richter, A., J. P. Burrows, H. Nüβ, C. Granier, and U. Niemeier: Increase in tropospheric nitrogen dioxide over China observed from space. *Nature*, **437**, 129−132, doi:10.1038/nature04092, 2005.

20   Roelle, P. A., Aneja, V. P.: Characterization of ammonia emissions from soils in the upper coastal plain, North Carolina. *Atmos. Environ*., **36**, 1087–1097, 2002.

Uno, I., Yumimoto, K., Pan, X. L., Wang, Z., Osada, K., Itahashi, S., Yamamoto, S.: Simultaneous dust–pollutants transport over East Asia: the Tripartite Environment Ministers Meeting March 2014 Case Study, *SOLA,* **13**, 47-52, doi:10.2151/sola.2017-009, 2017a.

25   Uno, I., K. Osada, K. Yumimoto, Z. Wang, S. Itahashi, X. Pan, Y. Hara, S. Yamamoto and T. Nishizawa: Importance of long-range nitrate transport based on long-term observation and modeling of dust and pollutants over East Asia, *Aerosol and Air Quality Research, **17**, doi:10.4209/aaqr.2016.11.0494,* 2017b.

Wang, Z., Pan, X., Uno, I., Li, J., Wang, Z., Chen, X., Fu, P., Yang, T., Kobayashi, H., Shimizu, A., Sugimoto, N., Yamamoto, S.: Significant impacts of heterogeneous reactions on the chemical composition and mixing state of dust

30   particles: A case study during dust events over northern China, *Atmospheric Environment*, **159**, 83−91, 2017a.

Wang, Z., Pan, X., Uno, I., Li, J., Wang, Z., Sugimoto, N., Yamamoto, S.: Modeling the long-range transport of particulate matters during winter in East Asia using NAQPMS and CMAQ, *Aerosol and Air Quality Research*, **17,** doi: 10.4209/aaqr.2016.12.0534, 2017b.

Xu, P. *et al*.: An inventory of the emission of ammonia from agriculture fertilizer application in China for 2010 and its high-resolution spatial distribution, *Atmos. Environ*. **115**, 141–148, 2015.

Yu, F. and Luo, G.: Modeling of gaseous methylamines in the global atmosphere: impacts of oxidation and aerosol uptake, *Atmos. Chem. Phys*., **14**, 12455-12464, doi:10.5194/acp-14-12455-2014, 2014.

5 Yumimoto, K., I. Uno, X. Pan, T. Nishizawa, S.-W. Kim: Inverse Modeling of Asian Dust Emission with POPC Observations for TEMM DSS 2014 Case Study, *SOLA,* **13**, 31−35, doi:10.2151/sola.2017- 006, 2017.

Zender, C. S., Bian, H., and Newman, D.: Mineral Dust Entrainment and Deposition (DEAD) model: Description and 1990s dust climatology, *J. Geophys. Res*., **108**(D14), 4416, doi:10.1029/2002JD002775, 2003.

Zhang, Q., Jiang, X., Tong, D., J. Davis, S.J., Zhao, H., Geng, G., Feng, T., Zheng, B., Zifeng, L., Streets, D.G., Ni, R.,
10   Brauer, M., van Donkelaar, A., Martin, R.V., Huo, H., Liu, Z., Da Pan, D., Kan, H., Yan, Y., Lin, J., He, K., and Guan, D.: Transboundary health impacts of transported global air pollution and international trade, *Nature* **543**, 705–709, doi:10.1038/nature21712, 2017.

Appendix

During the SVolc period (shown in Fig. 3), two typhoons passed south of Japan from east to west. Figure A1 shows snapshots of the trajectories and wind fields of Typhoon Halola (T12) and Typhoon Soudelor (T13), along with modeled SO_4^{2-} concentrations.

SO_4^{2-} in the northern part of Japan and Korea were under the control of long-range transport from China, while the southern part of Japan was covered by east winds (due to typhoons). This indicated that the high SO_4^{2-} concentrations in Fukuoka were due to Japanese domestic emissions and the impact of Mt. Sakurajima volcano (typically August 2−6). Note that the estimated SO_2 emission from Mt. Sakurajima is around 10^3 Gg year^{-1}, which is almost equivalent to the level of anthropogenic SO_2 emissions in Japan.

Figure A2 shows the volcano sensitivity experiment (VOFF) for SO_4^2. It is clear that the impact of the volcano was higher for the period August 2−6; during this period, SO_4^{2-} contributions converted from volcanic SO_2 emission exceeded 50% of the total SO_4^{2-}. Observations show higher values from July 27−August 1, and the model simulation failed to describe this. Volcanic emissions are natural phenomena and have strong day-by-day variation, so this failure of the model is due to underestimation of volcanic emissions during this period.

Table 1. Statistical summary of comparisons of the model results with observations between August 2014 and October 2015.

Concentration ($\mu g/m^3$)	Mean Observation ($\mu g/m^3$)	Mean Model ($\mu g/m^3$)	Normalized Mean Bias (NMB) (%)	Mean Fractional Bias (MFB) (%)	Mean Fractional Error (MFE) (%)	R
$PM_{2.5}$	17.51	11.26	-35.69	-46.71	53.68	0.72
PM_{10}	32.52	22.34	-31.31	-35.74	47.98	0.66
BC	0.64	0.44	-31.53	-38.77	61.64	0.35
fSO_4^{2-}	4.62	4.55	-1.53	-8.95	47.99	0.68
fNO_3^-	1.38	1.26	-8.47	-51.00	85.75	0.68
cNO_3^-	1.01	0.83	-18.16	-16.92	57.70	0.42

Table 2. Comparison of coarse-mode NO_3^- levels ($\mu g\ m^{-3}$)

Period	Observation	CTM			Mult. Regress. Analysis		
	cNO_3^-	$D\text{-}cNO_3^-$	$SS\text{-}cNO_3^-$	$Total\text{-}cNO_3^-$	$D\text{-}cNO_3^-$	$SS\text{-}cNO_3^-$	cNH_4
Jan.−June	1.29[a] (1.82)[b]	0.40	0.43	0.83	0.34	0.46	0.68
Sept.−Dec., July	0.94 (1.37)	0.06	0.73	0.79	0.11	0.50	0.26
Annual[c]	1.13 (1.61)	0.24	0.58	0.82	0.24	0.48	0.49

5 a ACSA observation.

   b D-F observation.

   c Average level between Sept. 2014 and July 2015 (excluding typhoon period).
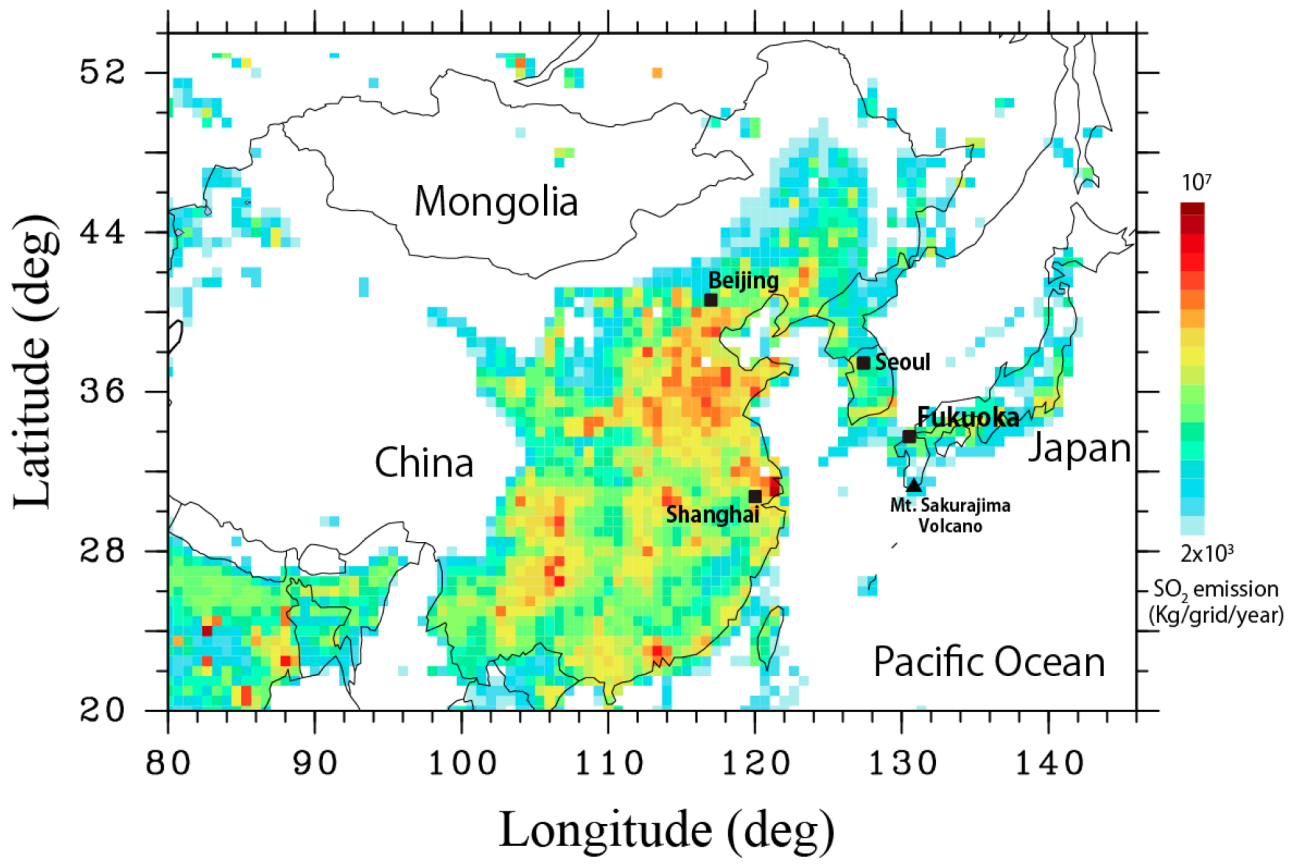
Figure 1. SO₂ emissions intensity (based on 2008 data) and observation sites: Fukuoka and Mt. Sakurajima volcano.
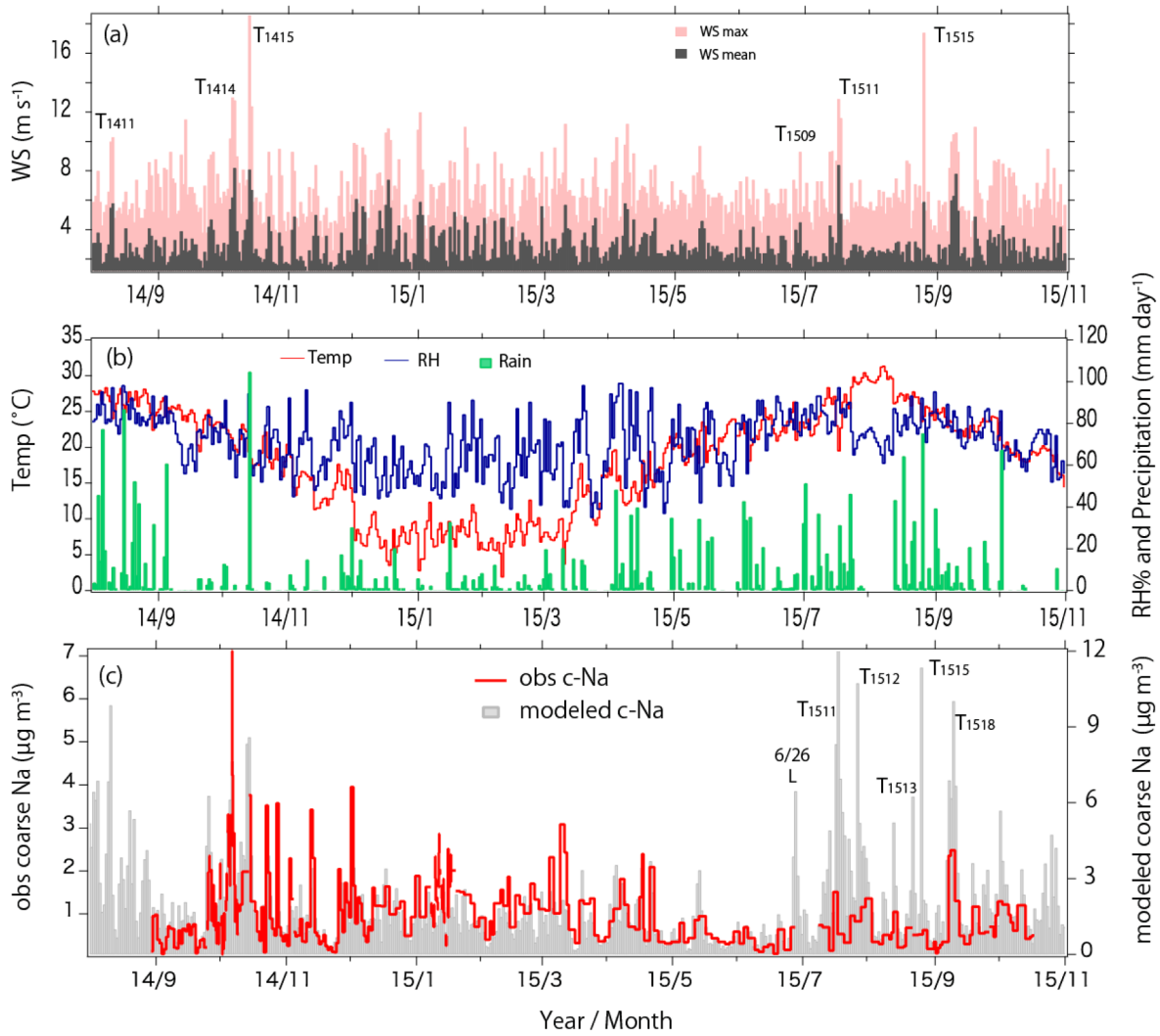
Figure 2. (a) Wind speeds (daily mean and maximum) at Fukuoka. (b) Daily average temperature, relative humidity (RH) and precipitation. (c) Observed coarse Na⁺ and modeled coarse Na⁺ (converted from GEOS-Chem coarse sea-salt (SALC)). T*yyxx* indicates typhoons: T1411 = Halong, T1414 = Fengshen, T1415 = Kalmaegi, T1509 = Chanhom, T1511 = Nangka, T1512 = Halola, T1513 = Soudelor, T1515 = Goni, T1518 = Etau.
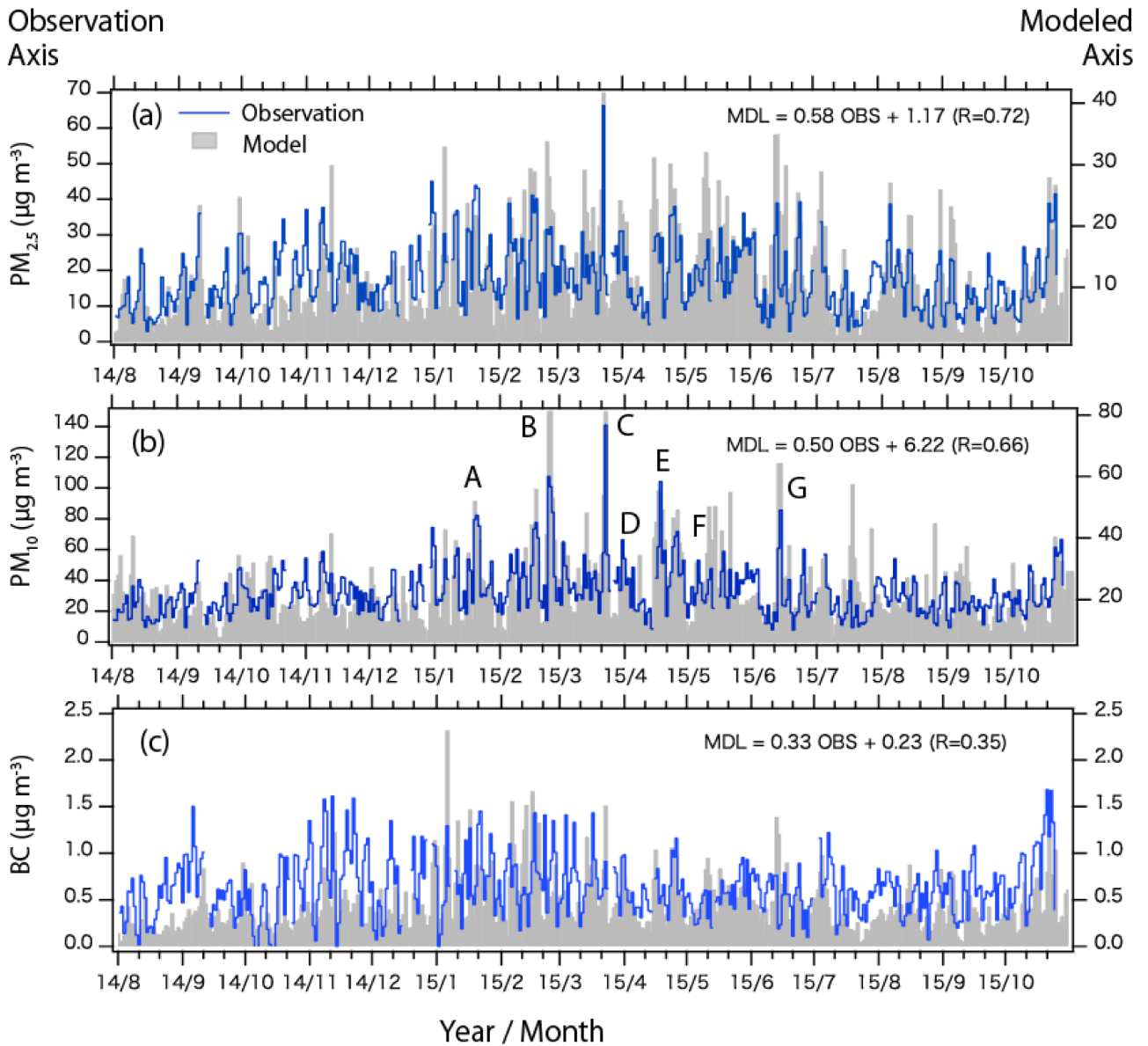
Figure 3. Daily average (a) particulate matter < 2.5 µm diameter (PM$_{2.5}$), (b) particulate matter < 10 µm diameter (PM$_{10}$), (c) black carbon (BC), (d) fine SO$_4^{2-}$, (e) fine NO$_3^-$, and (f) coarse NO$_3^-$. The blue line and dots show Aerosol Chemical Speciation Analyzer (ACSA) observations, the red line indicates measurements from the denuder filter pack (D-F) method, and gray shading indicates the model simulation. D-F data are sampling period averages. Observed data are on the left axis and numerical results are on the right axis, scaled by the regression results (except for c). Symbols A−G in (b) indicate major dust events in Fukuoka.
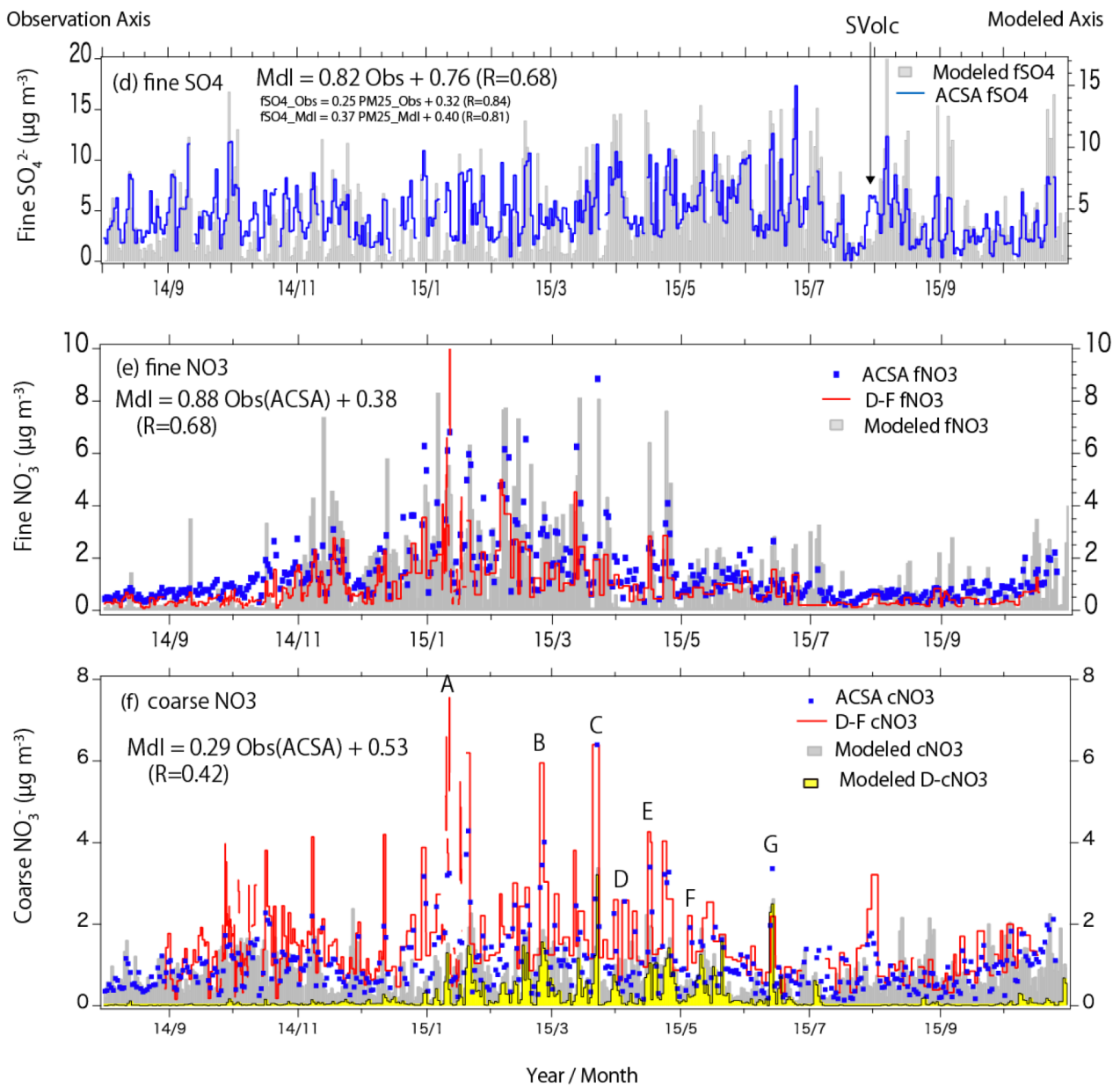
Figure 3. (continued)
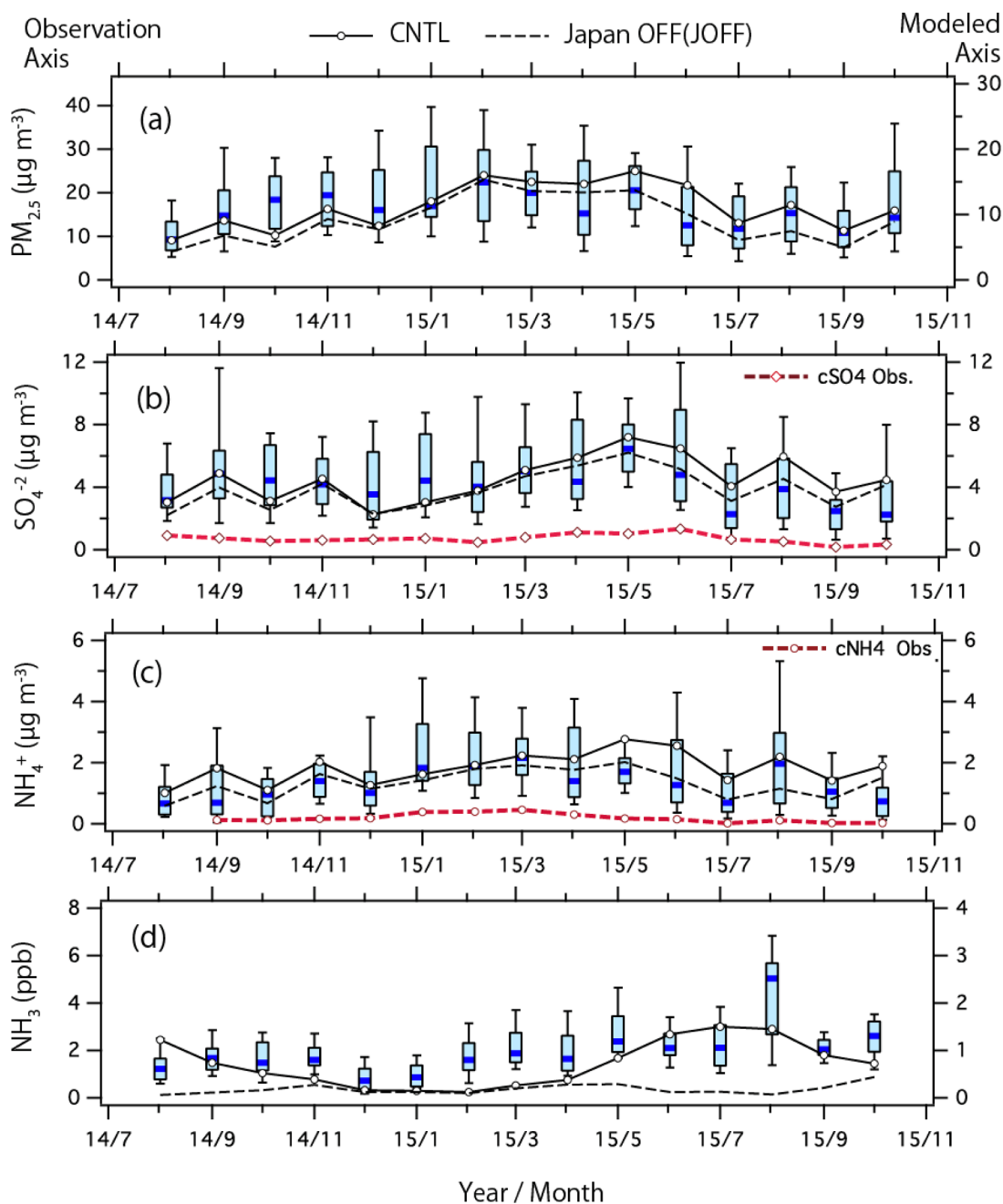
Figure 4. Monthly average plots of (a) PM$_{2.5}$, (b) fine SO$_4^{2-}$, (c) fine NH$_4^+$, and (d) NH$_3$ gas, (e) HNO$_3$, (f) total NO$_3^-$, (g) coarse NO$_3^-$, and (h) fine NO$_3^-$. Box-whisker plots show observations (10th, 25th, 50th, 75th, 90th percentile values). Red dashed-lines in (b) and (c) show ACSA-observed coarse mode concentrations. Black lines are modeled monthly averages; the straight line indicates the baseline model (CNTL), and the dashed line except (g) indicates the sensitivity experiment of Japanese emission reduction (JOFF). For (g), the dashed line shows the modeled dust-coarse NO$_3^-$ (D-cNO$_3^-$). HNO$_3$ observations are from D-F, and NO$_3^-$ observations are from ACSA.

Observation Axis   Modeled Axis
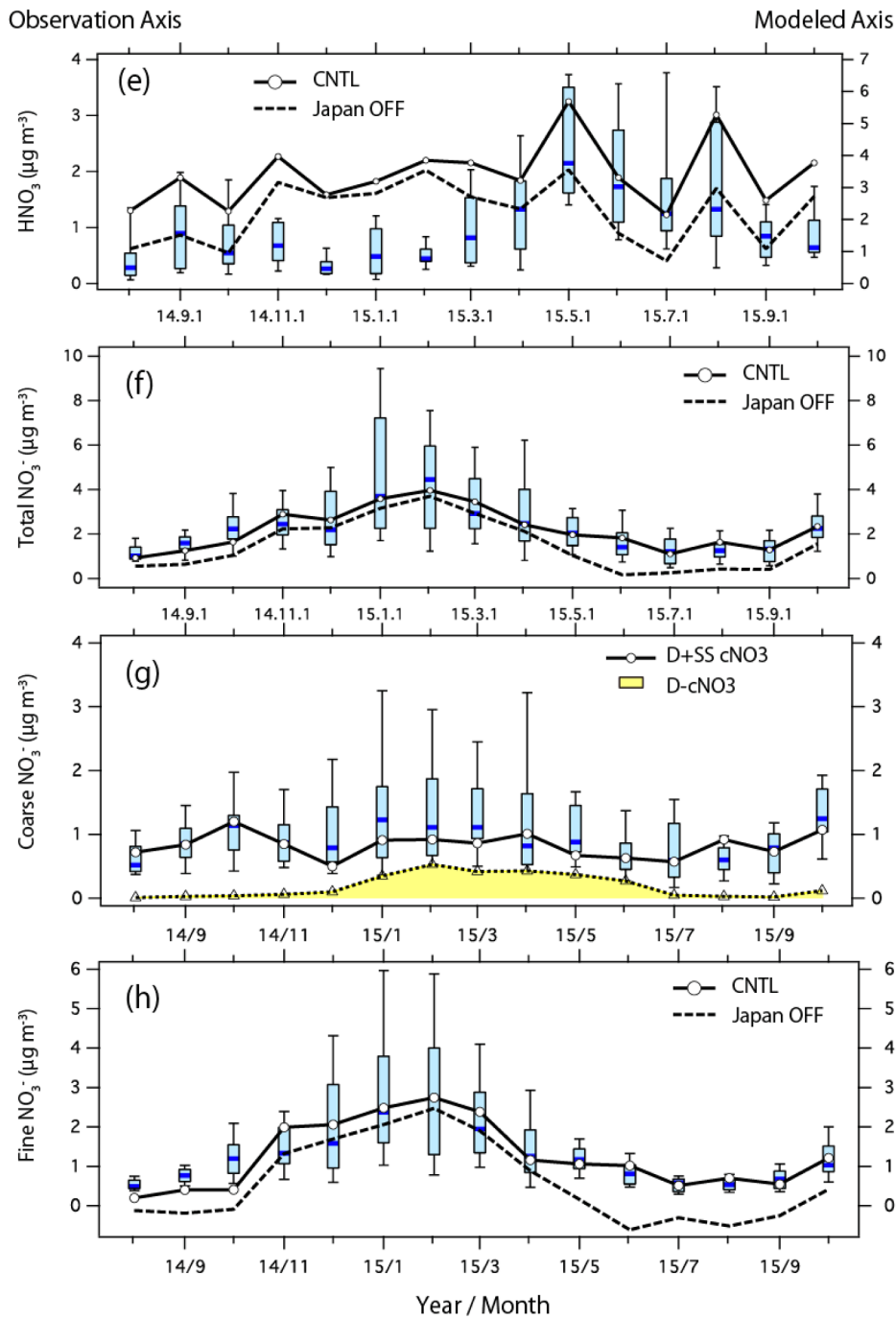
Figure 4. (continued)
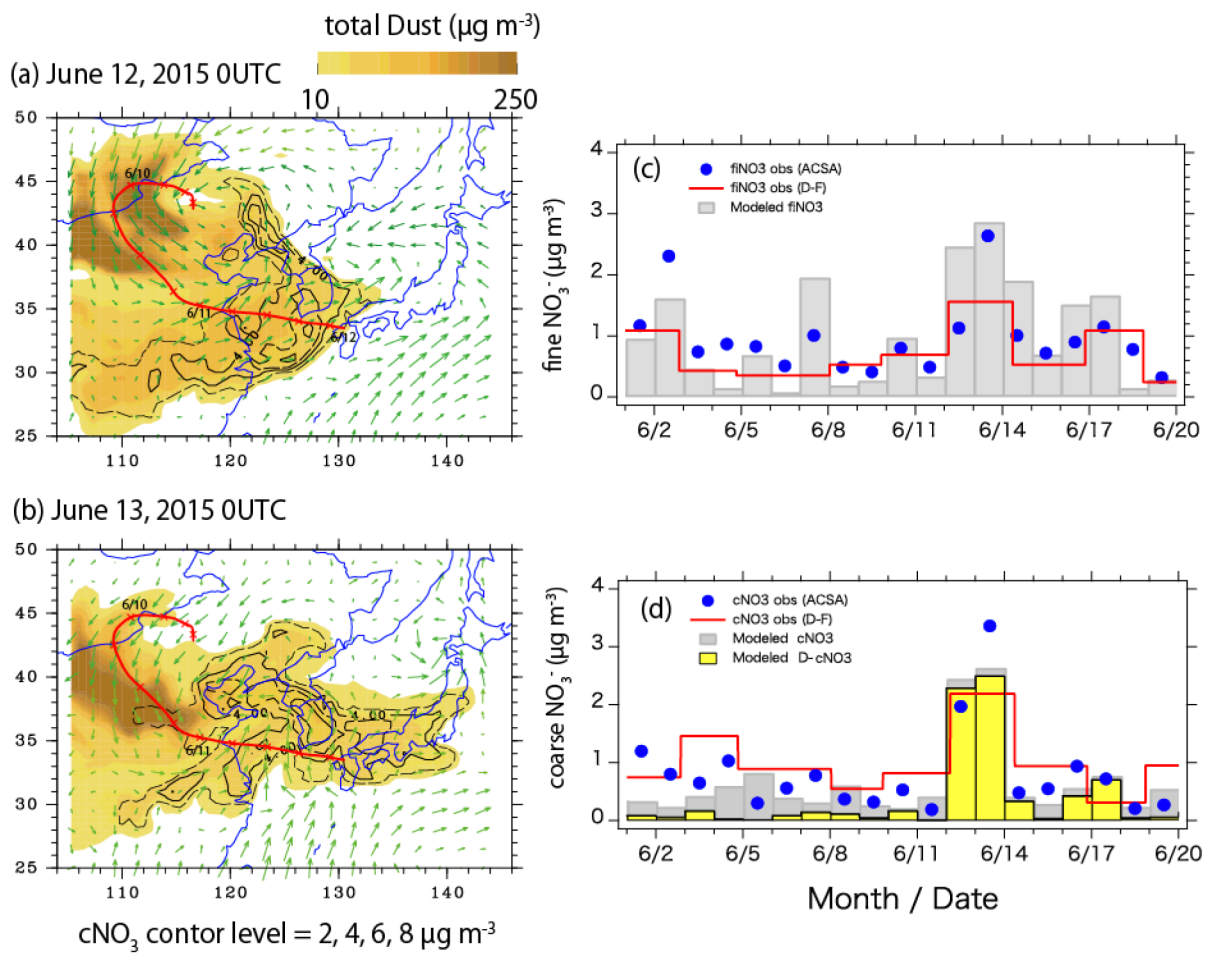
Figure 5. Horizontal distribution of dust (sum of all dust bins) (yellow color) and fine NO_3^- (contour) with wind vectors for (a) June 12, (b) June 13, and the time variation of daily average (c) fine NO_3^- and (d) coarse NO_3^-.
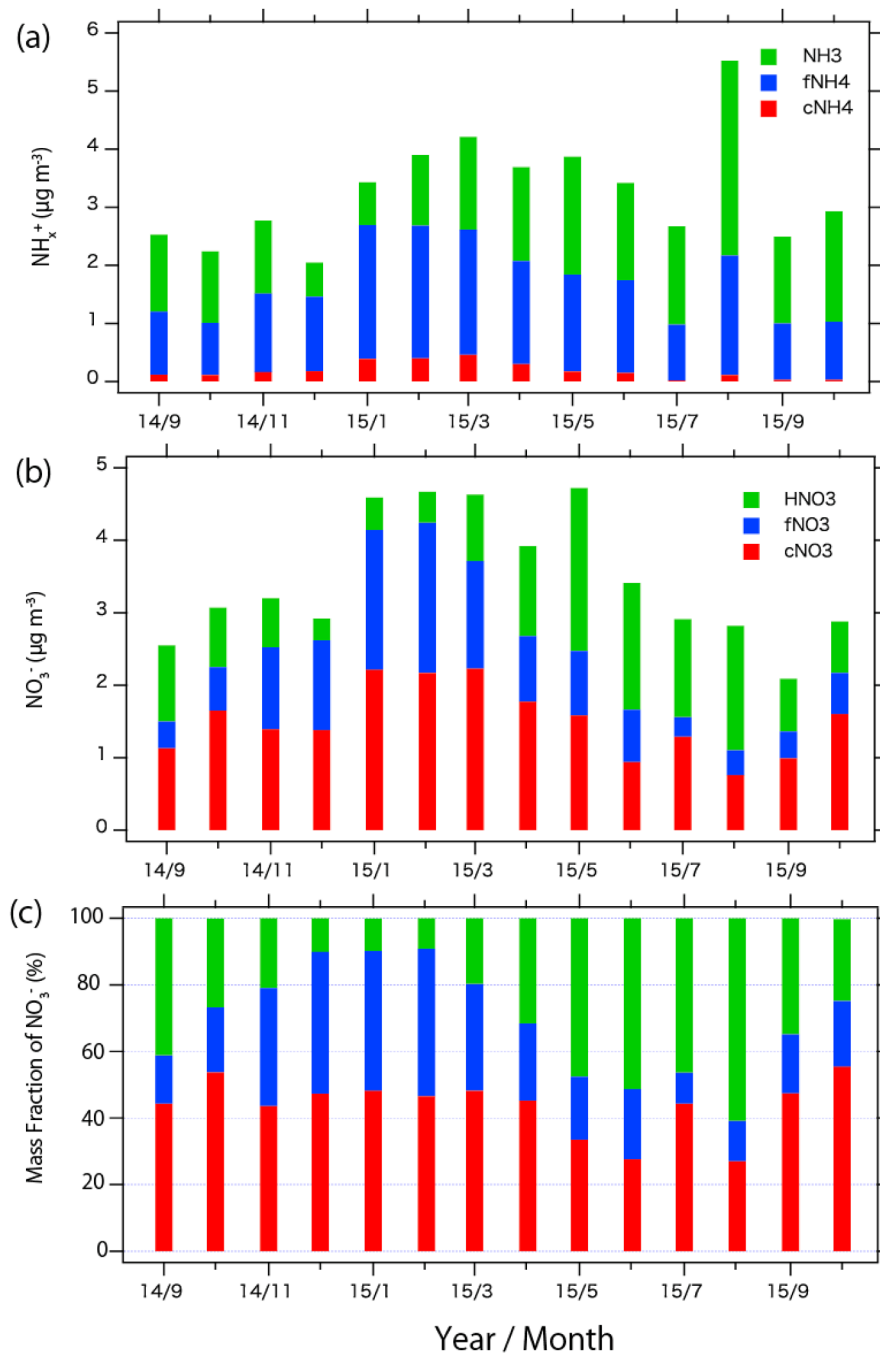
Figure 6. Monthly average values for (a) NHx, (b) NO₃, and (c) the mass fraction (%) of NO₃, observed by D-F.
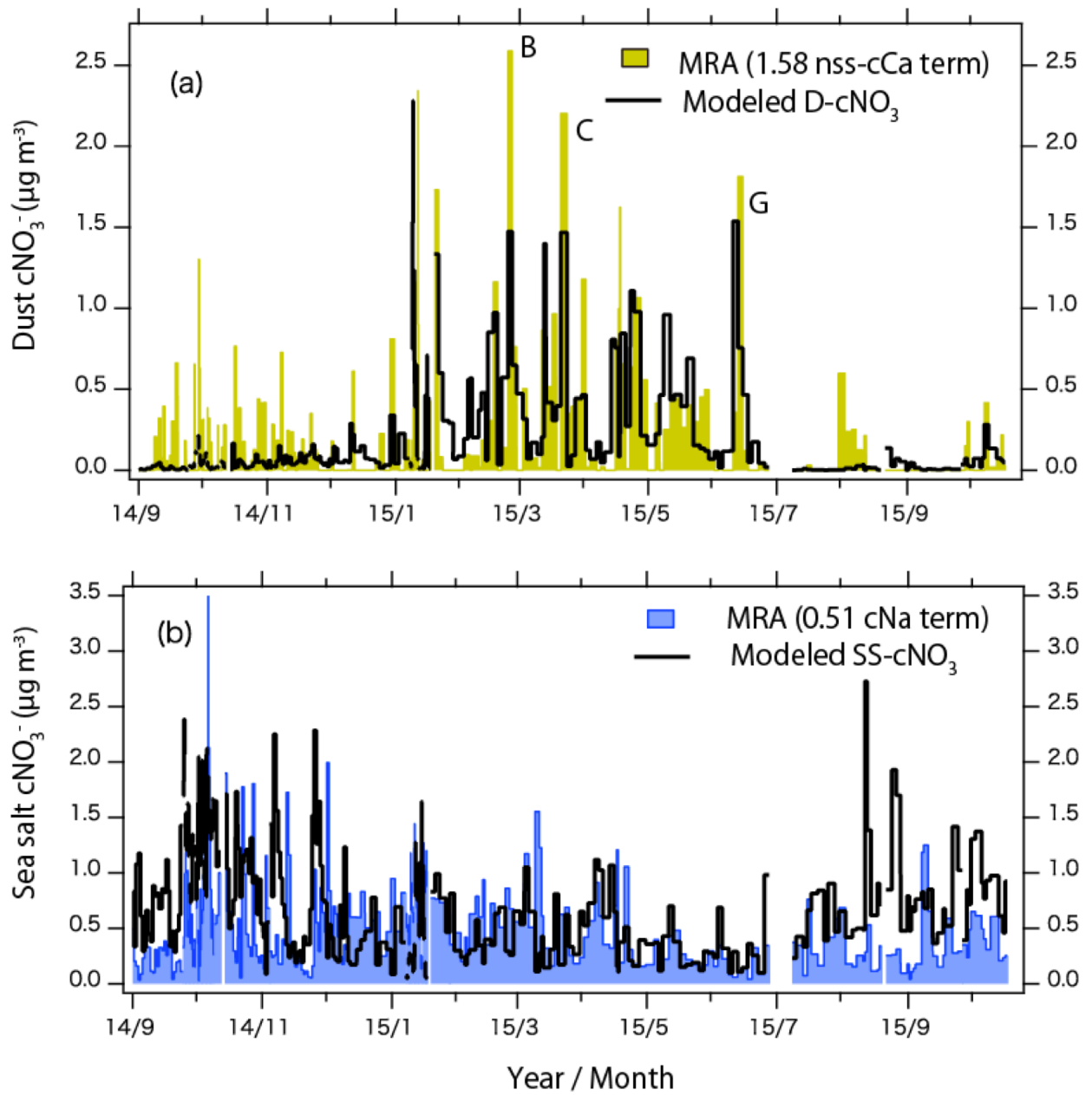
Figure 7. (a) D-cNO₃⁻ estimated by multiple regression analysis and modeled D-cNO₃⁻, (b) the same parameters for sea salt-NO₃⁻.
Modeled results averaged over the same time period as for the D-F measurements.
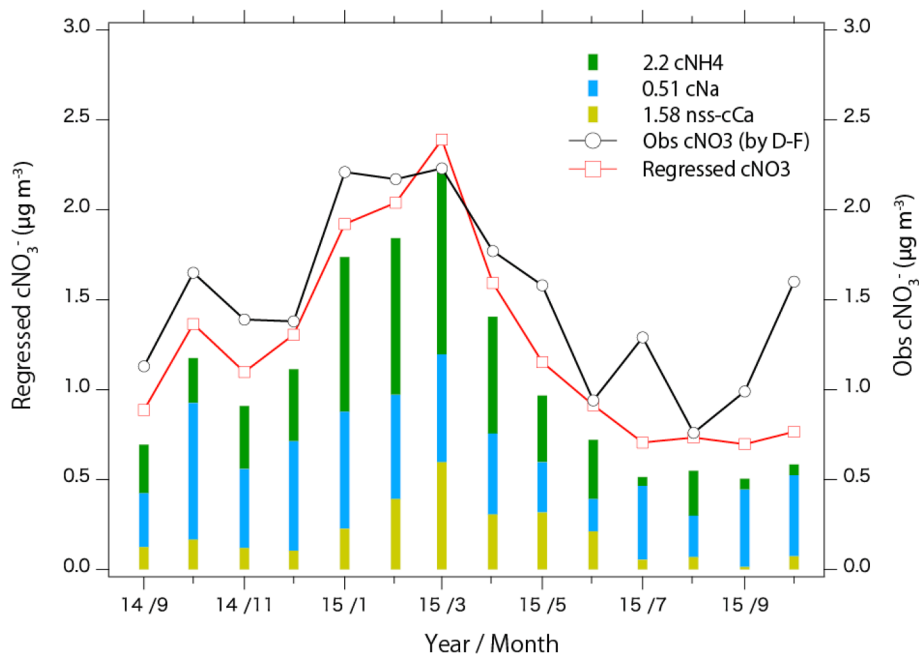
5   **Figure 8. Monthly average multiple regression results for the dust-cNO$_3^-$, sea salt-cNO$_3^-$, and cNH$_4^+$-related components.**
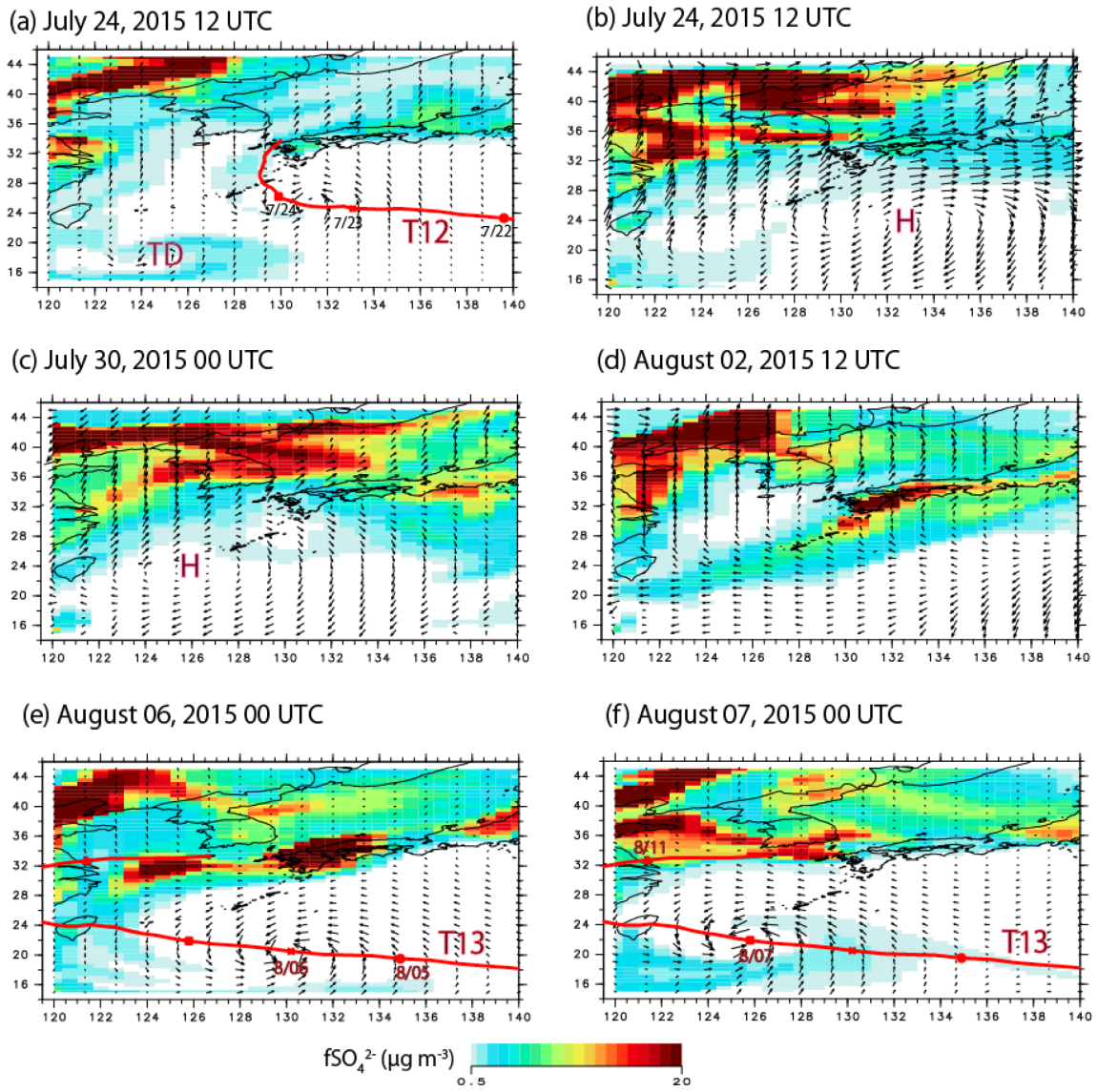
Figure A1. Horizontal distribution of fine SO$_4^{2-}$ (color) with wind vectors from model's first vertical level (65 m). The red line indicates the trajectory of Typhoon Halola (T12) in (a), and Typhoon Soudelor (T13) in (e) and (f).
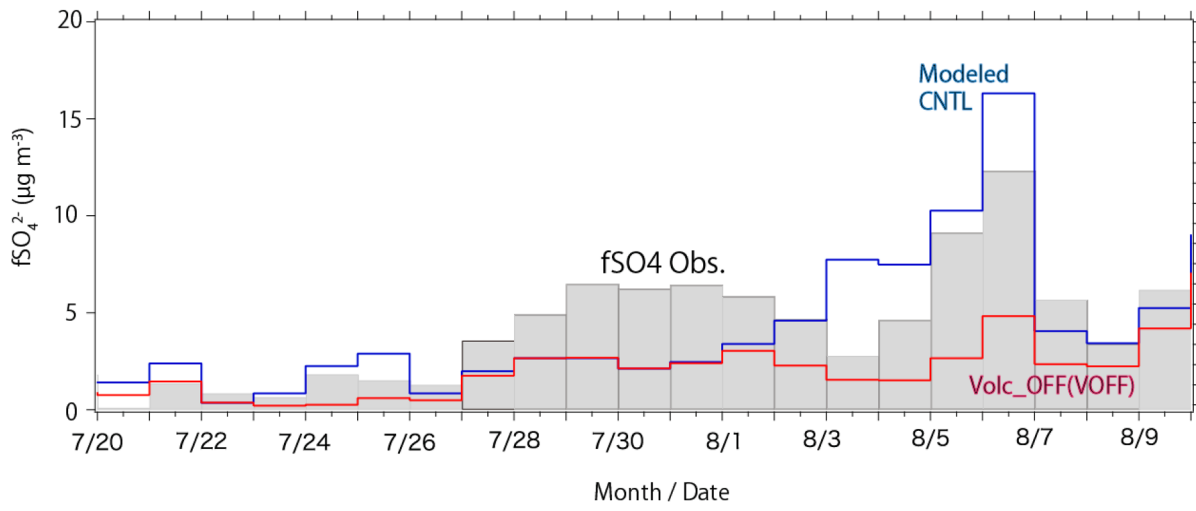
Figure A2. Daily average variation in observed (gray shading) and modeled fine SO$_4^{2-}$ (blue line = CNTL and red line = VOFF).